W/AlSiTiN_x/SiAlTiO_yN_x /SiAlO_x multilayered solar thermal selective absorber coating

A. AL-Rjoub[a,b,1], L. Rebouta[a], N. F. Cunha[a], F. Fernandes[c], N.P. Barradas[d,e], E. Alves[e]

a Centre of Physics, University of Minho, Campus de Azurém, 4800-058 Guimarães, Portugal

[b] SEG-CEMMPRE, Department of Mechanical Engineering, University of Coimbra, Rua Luís Reis Santos, 3030-788 Coimbra, Portugal

[c] Department of Control Engineering, Czech Technical University in Prague, Technicka 2, Prague 6 166 27, Czech Republic

d Centre for Nuclear Sciences and Technologies, DECN, IST, University of Lisbon, Bobadela, Portugal

e Institute for Plasmas and Nuclear Fusion, IST, University of Lisbon, Lisbon, Portugal

Abstract

Solar thermal energy has been used as a renewable green energy source. Here we present a design of highly selective solar thermal absorber coating deposited by dc magnetron sputtering, which is four layers based on W/AlSiTiN_x/SiAlTiO_yN_x/SiAlO_x. The coating revealed an excellent average solar thermal absorbance $\alpha = 95.5$ % with very low emittance $\varepsilon = 9.6$ % (calculated for 500 °C) together with an excellent thermal stability at 500 °C, in air for 350 h, and 630 °C in vacuum for 220 h.

Keywords: Selective coating, Sputtering, Thermal stability, AlSiTiN_x/SiAlTiO_yN_x

Introduction

Recently, there has been a significant increase in the levels of interest for the use of solar thermal energy as a renewable green energy source. For example, the concentrated solar power (CSP) is being used to produce the electricity by utilizing a parabolic-trough solar system, which concentrates the sunlight onto evacuated tubes containing a selective absorber coating. Then, the conducting heat can be used in steam turbines to produce electricity (Fernández-García et al., 2010) (Odeh et al., 1998) (Kalogirou et al., 1997). On the other hand, the cost of such generated electricity is relatively higher than the other resources. So, there is a need to improve the optical properties

[1] Corresponding author – e-mail address: abbaspl85@yahoo.com (A. AL-Rjoub)

and the thermal stability of the coatings' materials to be competitive with the other resources (Cagnoli et al., 2019). This can be done by improving the coatings' thermal stability such that operating at higher temperatures for longer terms (Rebouta et al., 2015), which can be achieved by smart selection of materials. Any design should have high solar absorbance (α) in the wavelength region of the solar radiation and very low thermal emittance in IR region (to minimize the energy losses by emission), good thermal stability and high oxidation resistance for long-term.

The current selective solar absorber coatings available in the market are two types: i) coatings based on metal-dielectric nanocomposite coatings (Cermet), which are multilayered coatings composed of a metal layer to improve the IR reflection as tungsten or molybdenum, interference absorber layers (high absorber (HA) and low absorber (LA)), finished with an anti-reflection (AR). As examples, the coatings based on Mo-Al_2O_3 (Zhang et al., 2006), Pt-Al_2O_3 (Nuru et al., 2012), WTi-Al_2O_3(Wang et al., 2017) and W-$AlSiO_x$ (Dias et al., 2017). ii) multi-layered designs based on transition metal nitrides and oxynitrides. This type showed a better thermal stability, oxidation resistance and perfect selectivity, which made them the most common recommended materials for the selective solar thermal absorbers used in CSP. The transition metal used in such coatings can be Ti (Barshilia et al., 2007) (Du et al., 2013) (Rebouta et al., 2012a) (Soum-glaude et al., 2017), Cr(Wang et al., 2019) (A AL-Rjoub et al., 2018), W (A. AL-Rjoub et al., 2018) (Dan et al., 2016), Nb (Y. Wu et al., 2015), and Al (Rebouta et al., 2015) or a combination between them. All of these optical stacks shared the designed structure as substrate\back-reflector metal\metal nitride\metal oxy-nitride\anti-reflection oxide layer.

In our previous work, designs of solar absorber coatings based on nitride/oxynitride layers (W/CrAlSiN_x/CrAlSiO_yN_x/SiAlO_x)(A. AL-Rjoub et al., 2018) and with structure (W/WSiAlN_x /WSiAlO_yN_x/SiAlO_x) (A. AL-Rjoub et al., 2018) were studied. In this study we present a design of highly selective solar thermal absorber coating based on W/AlSiTiN_x/SiAlTiO_yN_x/SiAlO_x for high temperature applications.

1. Methods and experimental details

1.1 Materials: the materials used in this coating include: a) Several targets of 10 cm in diameter with purity 99.99% as Ti50Al50 at% with 9 silicon pellets of 10 mm diameter added on the target erosion zone (used to obtain the AlSiTiN_x and SiAlTiO_yN_x layers), Si80Al20 at% (used to produce the oxide anti-reflection layer of the stacks) and W target which was used for the back-

reflector coating. b) Oxygen and nitrogen as reactive gases, and argon as sputtering gas. c) Glass, p-doped Boron Si (100) mirror polished wafer and well-polished stainless-steel (AISI304) substrates. d) Acetone and ethanol for substrate cleaning.

1.2 Experimental description: All coatings were produced at room temperature by dc-magnetron sputtering with argon working pressure of 0.37 Pa, applied current density of 6.4 mA/cm^2, pulsed bias of -60 V and base pressure of 2×10^{-4} Pa), except the tungsten layer where the used current density was 12.7 mA/cm^2. Glass substrates were cleaned by ethanol, whereas the silicon and stainless-steel substrates were cleaned in acetone by ultra-sound 10 min and by ionic etching. Several single layers of $AlSiTiN_x$ and $SiAlTiO_yN_x$ were deposited on substrates of glass with changing the nitrogen and oxygen gasses flow, which used in simulation of the optical constants and thickness. Thicker single samples similar to those in the final tandem were produced on silicon and on stainless-steel substrates to study their morphology, chemical composition and structural. The tandem was applied to annealing tests in air at 500 ºC for 350 h and in vacuum at 630 ºC for 220 h.

1.3 Optical constants and simulated thicknesses: the refractive index (n), extinction coefficient (k) and thicknesses of thin $AlSiTiN_x$ and $SiAlTiO_yN_x$ layers were obtained from SCOUT software (version 2.99, WTheiss Hardware and Software) simulation after measuring their transmittance (T) and reflectance (R), using a Shimadzu PC3100 spectrophotometer, in the wavelength range of 0.30 – 2.5 µm as completely described in our previous studies (A. AL-Rjoub et al., 2018) (A. AL-Rjoub et al., 2018).

1.4 Chemical composition, structural analysis and chemical-bonding of coatings: EDS with 10 keV accelerated voltage was used to evaluate the chemical composition of the coatings, and cross-section SEM images of the coatings was used to study the morphology and thicknesses calculations.

Structure and coatings' thermal stability in as deposited and after annealing was studied by X-ray diffraction (XRD) and by the Rutherford Backscattering (RBS) (Barradas and Jeynes, 2008).

The chemical-bonding states of individual thick layers of $AlSiTiN_x$ and $SiAlTiO_yN_x$ was investigated by using X-Ray Photoelectron Spectroscopy (XPS), taking in the account the C1s line at 285.0 eV to calibrate the binding energies and the spectra were fitted by CasaXPS software (version 2.3.19, Casa Softw. Ltd). The Ti 2p core level was fitted considering the peak doublets spin-orbit separation (ΔE_P) $2p_{1/2} - 2p_{3/2}$ as 5.7 eV, 6.0 eV and 6.1 eV for oxides, nitrides and metal states, respectively. with peaks' intensity ratio $\frac{I_{Ti\,2p_{1/2}}}{I_{Ti\,2p_{1/2}}} = 0.5$ (Biesinger et al., 2010) (Rahman et al., 2016).

2. Results and discussion

2.1.1 Single layers

The back reflector tungsten and the antireflection $SiAlO_x$ layers were studied in detail in our previous studies (Dias et al., 2017) (A. AL-Rjoub et al., 2018) (A. AL-Rjoub et al., 2018). So, here only $AlSiTiN_x$ and $SiAlTiO_yN_x$ are presented.

2.1.2 Optical properties of single layers $AlSiTiN_x$ and $SiAlTiO_yN_x$

Several $AlSiTiN_x$ and $SiAlTiO_yN_x$ thin single layers were deposited on glass substrates with different nitrogen partial pressures ranged from 0.017 to 0.041 Pa, in the case of $AlSiTiN_x$, and with oxygen and nitrogen partial pressures ranged from 0.053 to 0.085 Pa in the case of $SiAlTiO_yN_x$. The optical constants n and k of those layers were simulated from their experimental reflectance and transmittance measurements with the help of SCOUT software. As shown in Fig. 1, n and k decreased as the partial pressures of the gases increased in both nitrides and oxynitrides layers, due to the loss of their metallic behavior and due to the formation of transparent nitrides and oxides of Al and Si. Also, the refractive indices of $AlSiTiN_x$ increased in the wavelength range of 300 – 1000 nm, which improves the solar absorption thus enhancing through the interference effect (Yin and Collins, 1995). The refractive indices of $SiAlTiO_yN_x$ layers behave similarly in lower gas partial pressure and become constant for higher gas partial pressures.

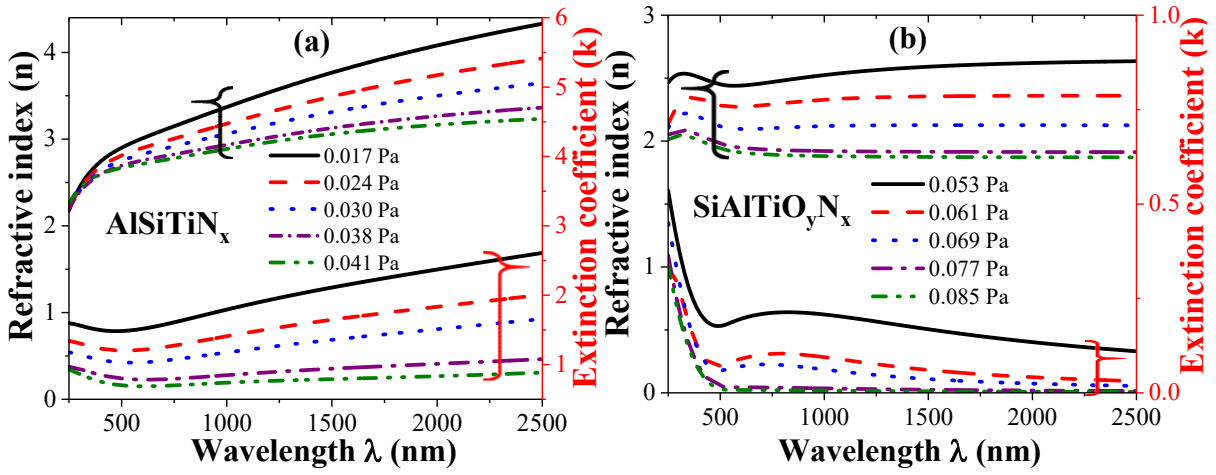

Fig. 1: n and k as a function of wavelength of: (a) $AlSiTiN_x$ and (b) $SiAlTiO_yN_x$, prepared with different reactive gases partial pressures.

2.1.3 Chemical-composition of single layers

The chemical composition of $AlSiTiN_{P= 0.038\ Pa}$ and $SiAlTiO_yN_{xP= 0.069\ Pa}$ thick layers similar to the one used in the final absorber stack were evaluated by EDS and the results are presented in Table I. From nitride to oxynitride a strong increase of oxygen was found, as expected. A small decrease was found for aluminum and titanium at%, but in contrast a small increase in Si content was found. This is due to the effect of the addition of oxygen as a reactive gas, which induced a stronger target poisoning effect on Al and Ti than on Si, decreasing the relative sputtering yield of Al and Ti in comparison to Si, resulted in an increase of Si content. These differences explain why $AlSiTiN_{P= 0.038\ Pa}$ has higher optical constants than $SiAlTiO_yN_{xP= 0.069\ Pa}$ and as a result high and low solar thermal absorber layers, respectively.

Table I: The chemical composition of $AlSiTiN_{P= 0.038\ Pa}$, $SiAlTiO_yN_{xP= 0.069\ Pa}$, thick layers deposited on stainless-steel.

Layer	N at%	O at%	Al at%	Si at%	Ti at%	Ar at%
$AlSiTiN_{P=0.038\ Pa}$	33	-	26	22	17	2
$SiAlTi(ON)_{P=0.069\ Pa}$	16	22	22	25	12	3

In order to evaluate the chemical bonding states, another individual samples of $AlSiTiN_{P= 0.038\ Pa}$ and $SiAlTiO_yN_{xP= 0.069\ Pa}$ similar to the used in the multilayered designs were surveyed by XPS. Fig. 2 shows the spectral core level of Ti 2p, N 1s, Si 2p and Al 2p. Fig. 2a shows the Ti 2p core level spectra, which show an evidence of the existence of different titanium oxidation states in both samples. These peaks were divided into three doublet components considered as Ti $2p_{3/2}$ and Ti 2 $p_{1/2}$. The Ti $2p_{3/2}$ peaks centered at 455.4, 457.3 and 459.0 eV can be corresponded to Ti(Al)-N, Ti-O-N and Ti-O bonds (Zhang et al., 2017) (Zhao and Wackelgard, 2006)(Wainstein and Kovalev, 2018) (Chen et al., 2019) (Rahman et al., 2016) (Chen et al., 2019) (Z. L. Wu et al., 2015), respectively. In the nitride sample ($AlSiTiN_{P= 0.038\ Pa}$), the Ti $2p_{3/2}$ peak at 453.9 eV corresponds to the Ti atoms in metallic oxidation state (Biesinger et al., 2010) (Z. L. Wu et al., 2015), which disappeared in the case of $SiAlTiO_yN_{xP= 0.069\ Pa}$ sample.

The core level of N 1s can be deconvoluted into three peaks in the two samples as shown in Fig. 2b. The peaks centered at energies 396.5, 397.5 and 399.0 eV associated to Ti(Al)-N, Si-N and Si-O_3N compounds, respectively(Oliveira et al., 2015) (Zhang et al., 2017) (Rahman et al., 2016) (A. AL-Rjoub et al., 2018).

Fig. 2c the Si 2p core-level, where the two specimens have the common three peaks located at 100.6, 101.7 and 102.6 eV, which they recognized as Si(Al)-Si_2N_2, Si_3N4 and Si-O-Al, respectively (Oliveira et al., 2015) (Costa et al., 2018)(Rebouta et al., 2015) (AL-Rjoub et al., 2017). The fourth peak of nitride sample ($AlSiTiN_{P= 0.038\ Pa}$) centered at 98.7 is considered as Si elemental bond (Z. L. Wu et al., 2015) (Oliveira et al., 2015).

Finally, Al 2p core level is shown in Fig. 2d, the two samples share the components centred at 73.9 and 74.8 eV related to Ti(Al)-N and Al-O, respectively(Z. L. Wu et al., 2015) (Wainstein and Kovalev, 2018) (Costa et al., 2018) (Rahman et al., 2016).

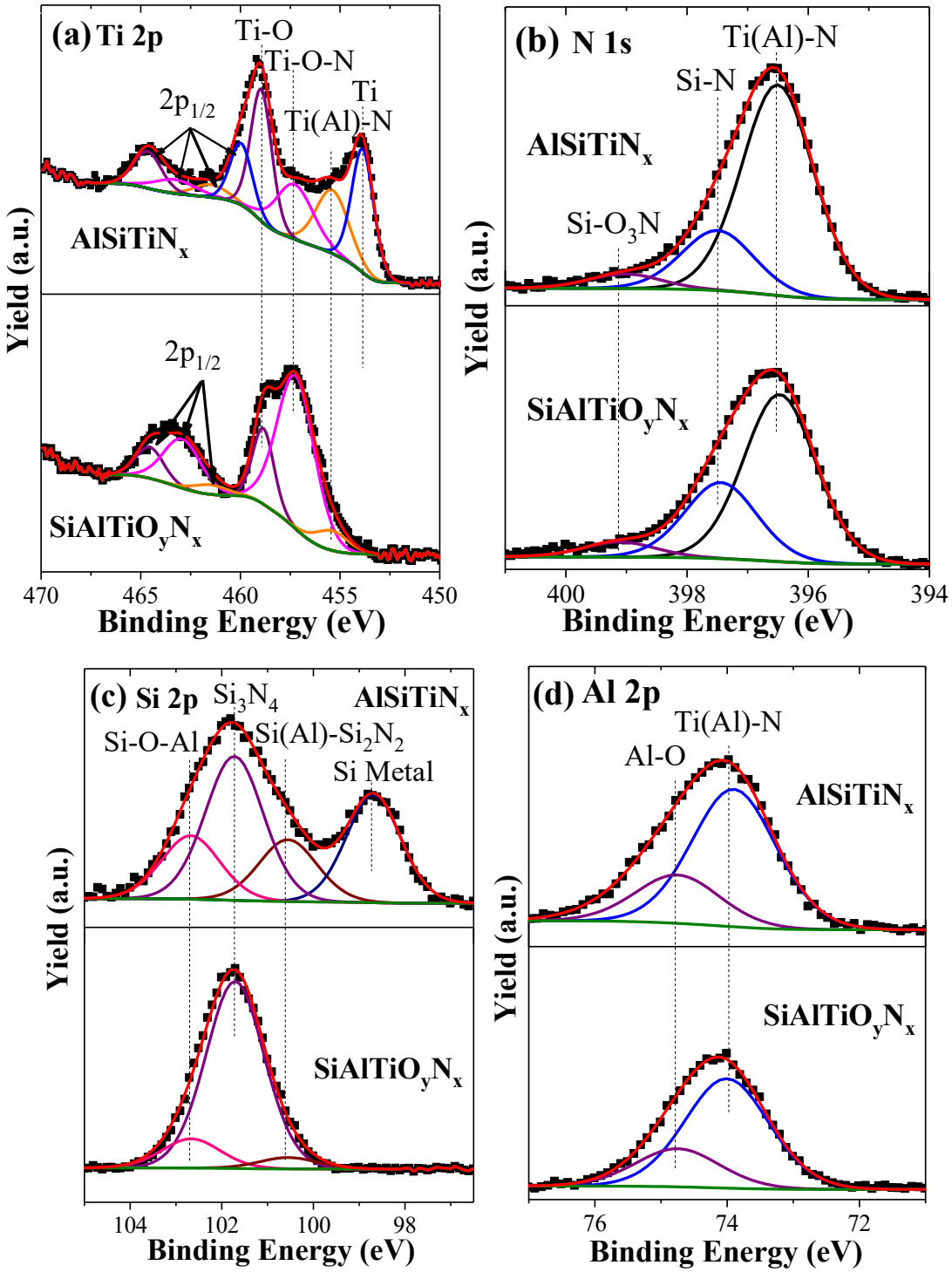

Fig. 3. XPS-spectra of: (a) Ti 2p, (b) N 1s, (c) Si 2p, (d) Al 2p core level of $AlSiTiN_{P=\ 0.038\ Pa}$ and $SiAlTiO_yN_{xP=\ 0.069\ Pa}$ single layers. The green line in figures is the background correction.

158 ### 2.1.4 Morphology and crystalline structure of single layers

159 Thick individual layers of $AlSiTiN_{P=0.038\ Pa}$ and $SiAlTiO_yN_{xP=\ 0.069\ Pa}$ deposited on stainless steel
160 substrates were used to study their crystalline structure by X-ray diffraction (XRD). Both samples
161 are amorphous as also no features appears in SEM as presented in Fig. 3.

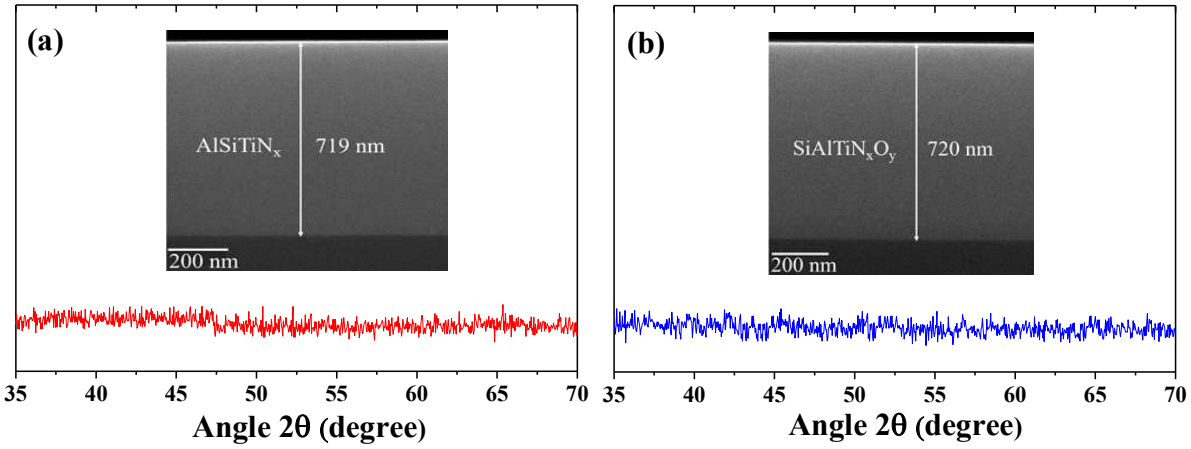

162

163 **Fig. 3:** XRD-pattern and cross-section SEM images of: a) $AlSiTiN_{P=\ 0.038\ Pa}$ and b) $SiAlTiO_yN_{xP=\ 0.069\ Pa}$ thick
164 single layers.

165 ### 2.2 Multilayer Design

166 The multilayer stack coatings were previously modelled by SCOUT-software depending on
167 their single layers' information, that allows the calculation of their optical constants n and
168 extinction k as a function of wavelength, together with their thicknesses. Then the structure and
169 the reflectance curve of the final stack was simulated, and deposited on 304 stainless-steel
170 substrates. The experimental total reflectance of the stack was also measured and as shown in Fig.
171 4a.

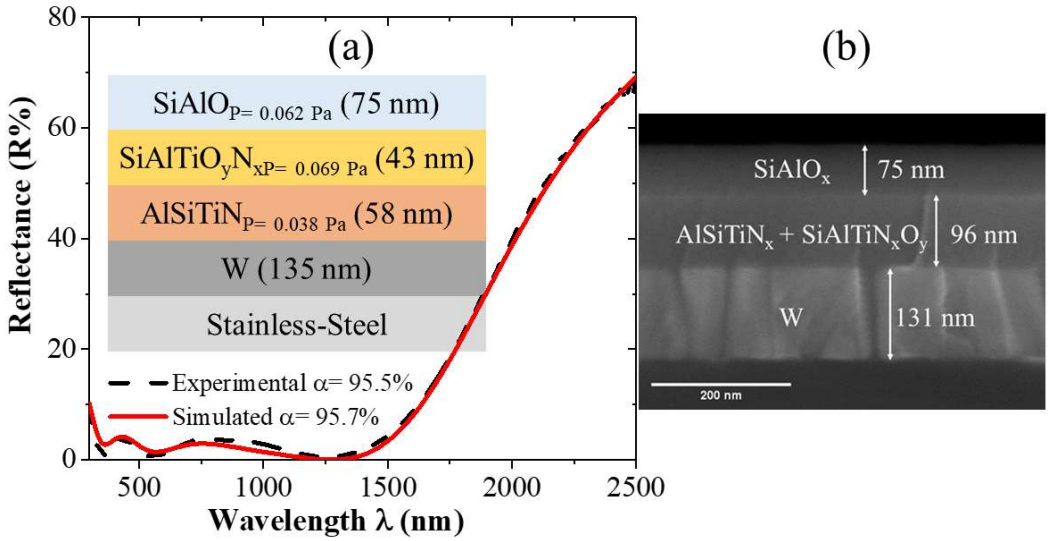

Fig. 4: (a) Schematic-diagram of the simulated optical tandem with corresponding simulated and experimental reflectance curves. (b) SEM Cross-section SEM image of the multilayered coating optical tandem.

As it is also displayed in Fig. 4a, the tandem is a multilayer composed of four layers: i) the tungsten layer, with thickness ~ 131 nm as back-reflector to improve the whole reflectance in IR wavelength region. ii) $AlSiTiN_x$ /$SiAlTiO_yN_x$ two absorption structural layers, which they are undistinguishable in the SEM image. iii) $SiAlO_x$ as antireflection protective layer, which is protect the inner layers and allow the light to pass through. The reflectance of as deposited tandem is in agreement of the simulated one and has a thickness of ~ 301 nm, and it shows a very high solar absorptance, α= 95.5 % with very low emissivity, ε= 9.6 % (calculated for 500 ºC using the IR reflectance measurements) and ε= 7.8 %, when calculated for 400 ºC, simultaneously.

2.3 Thermal stability

The thermal stability and oxidation resistance of the tandems were tested by subjecting them to annealing tests in air, at 500 ºC, and in vacuum, at 630 ºC, for 350 h and 220 h, respectively. After each step of annealing, the absorptance (α) and the thermal emittance (ε) were calculated from the reflectance curves. Fig. 5a shows the reflectance curves of as deposited, after 50 h and after 350 h air annealing, with their solar absorptance and thermal emittance at 500 °C after each step shown in the legend. As seen in the figure, the coatings show an excellent thermal stability and no changes reported in the reflectance curve, solar absorptance and thermal emittance values in the second annealing step (of 350 h), which reflect a very good thermal stability. However, after the first step of annealing, small changes in the reflectance curve especially for wavelengths greater than 2000

nm due to tungsten phase structure change (α and β phases), which is normal and fully studied in the previous studies (AL-Rjoub et al., 2019) (Chen et al., 2005) (O'Keefe and Grant, 1996) (Antonaia et al., 2010). The vacuum annealing was performed in two steps, 20 h and 220 h, as shown in Fig. 5b, the tests insure a very good thermal stability. Although those results were obtained at higher testing annealing temperatures in air and in vacuum than the one of the coating based on AlSiOx:W(Dias et al., 2017), WSiAlN x/WSiAlOyNx(A. AL-Rjoub et al., 2018) and/or $CrAlSiN_x/CrAlSiO_yN_x$(A AL-Rjoub et al., 2018) (Al-rjoub et al., 2019), they showed better thermal stability. Moreover, the emittance values calculated at 400 ºC of this design is lower than the later.

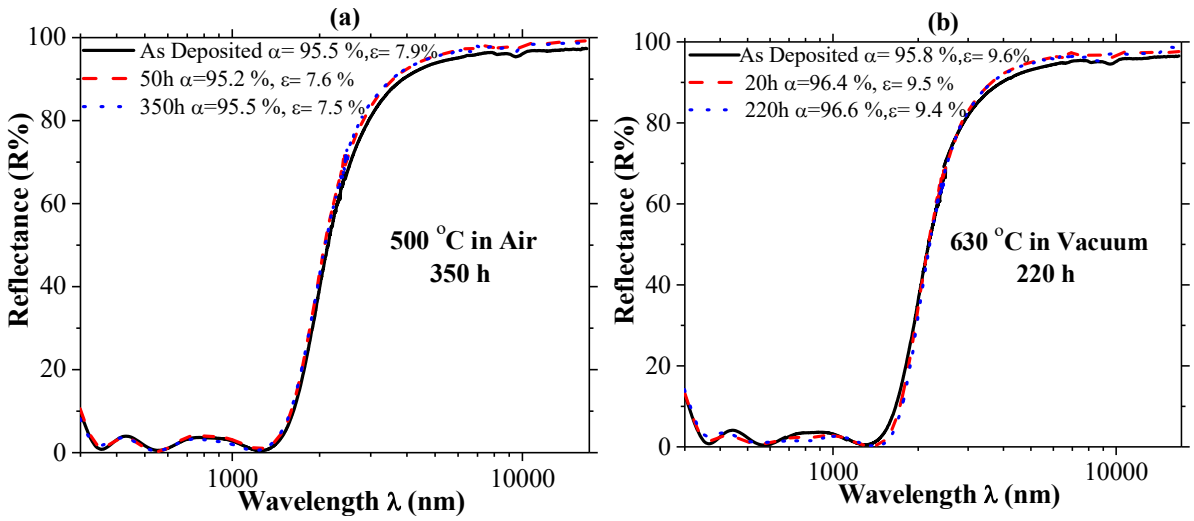

Fig. 5: the reflectance curves of as deposited tandems and after annealing (a) in air at 500 ºC (b) in vacuum at 630 ºC, with measured values of the solar absorptance (α) and the thermal emittance (ε) (calculated for 500 ºC).

Rutherford back scattering (RBS) was also used to study the elemental depth profiles of the absorbers, as shown in Fig. 6. It shows three optical stack coatings deposited in same run and subjected to different thermal annealing, namely as deposited, after air annealing at 500 ºC for 350 h and after vacuum annealing at 630 ºC for 220 h. The composition of elements was determined from their front edges because of the signals can overlap as indicated in the figure. The analysis shows that the three as deposited samples have a small difference in the thickness of W layer. The relative heights of these front edges are correlated due to the relative concentrations of the different elements, and the position of the different elements, if located at surface sample, are indicated in the graph. It is difficult to distinguish between silicon and aluminum

because they have very close atomic masses. Nevertheless, the analysis shows a small difference between as deposited and vacuum annealed samples. After air annealing no changes were recorded for the coating reflecting an excellent thermal stability against diffusion and oxidation. For annealing in vacuum, a small changes of W depth profile were seen due to its small elemental diffusion to the stainless-steel substrate, which can be easily solved by adding a barrier layer as shown in the previous study (AL-Rjoub et al., 2019).

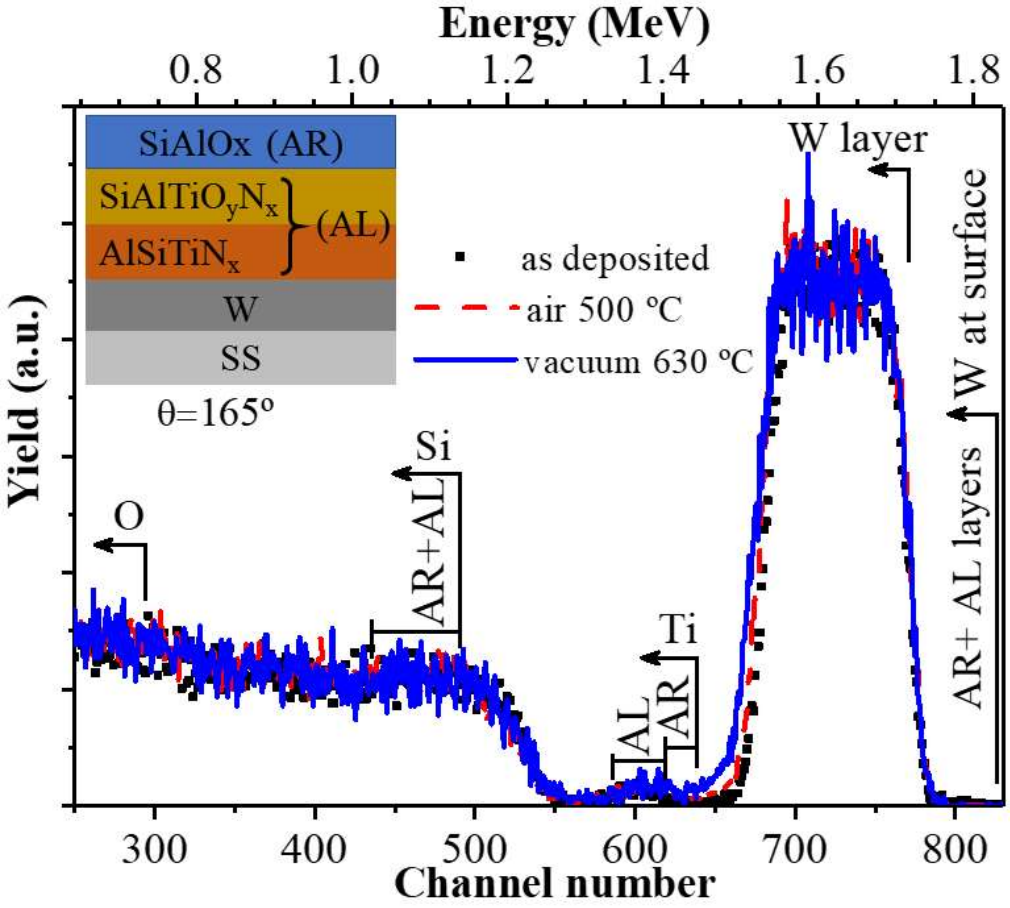

Fig. 6**:** The spectra of RBS of the stacks as deposited and after air thermal annealing at 500 ºC and vacuum thermal annealing at 630 ºC for 350h and 220 h, respectively.

Further structural tests were applied on the coatings after the thermal treatments using XRD to analyze if it whether or not it has some changes due oxidation. Fig. 7 shows the XRD diffractograms of the three samples (as deposited, after air and vacuum annealing). As shown in the figure, no changes have been recorded after the thermal treatment , except small differences in the stainless-steel peaks and in the intensity of W peaks, which reflecting that the coatings showed a very good oxidation resistance and its thermally stable after annealing in air and vacuum at 500

ºC and 630 ºC, respectively. The W recrystallization induced by the thermal annealing also contribute to the tungsten phase structure change (AL-Rjoub et al., 2019) (Chen et al., 2005) (O'Keefe and Grant, 1996) (Antonaia et al., 2010), which is related with the reflectance increase in the infrared wavelength range resulting in a consequent emissivity decrease. The W grain sizes were calculated from the full width at half maximum (FWHM) of (110) tungsten peak and using the Scherrer equation, in as deposited state and after annealing. The grain size of as deposited sample was 21.4 nm, and a slight increase was found, 24.6 nm and 26.4 nm after the annealing in air, at 500 ºC, and in vacuum, at 630 ºC, respectively.

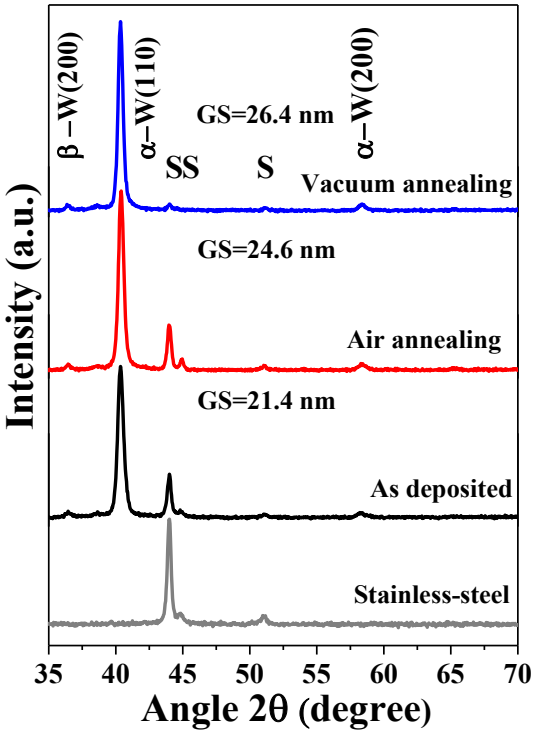

Fig. 7: X-ray diffraction of tandems before and after thermal annealing.

The structure based on $AlSiTiN_x/SiAlTiO_yN_x$ showed better performance than the structure based on $TiAlN_x/TiAlO_yN_x$ (Barshilia et al., 2007) (Rebouta et al., 2012b) (Du et al., 2013). In general the structure based on Me1(Me2)SiN/Me1(Me2)SiON, where Me1 is a transition metal element and Me2 is Al or another transition metal, revealed better performance than those based on Me1(Me2)N/Me1(Me2)ON. This behaviour was also reported for CrAl (A AL-Rjoub et al., 2018) (Al-rjoub et al., 2019), Cr (Zou et al.,

2015)and NbTi(Y. Wu et al., 2015), which means that the Si addition improves the thermal and chemical stability.

Silicon usually assumes fourfold coordination and transition metal in respective nitrides (fcc lattice) are six fold coordinated, and with high surface mobility during the deposition, Si atoms are segregated, allowing the nucleation of the SiN_x phase, which forms a layer on the growth surface covering the nitride nanocrystallites and limiting their growth, resulting in a two phase material with improved properties(Vepfek and Reiprich, 1995) (Veprek and Veprek-heijman, 2008) . Thus, the oxidation resistance and barrier diffusion properties of transition metal nitrides and transition metal oxynitride films can be improved by the addition of Si (Vepfek and Reiprich, 1995) (Thobor-keck et al., 2005) (Kim et al., 2006) (Najafi et al., 2013)

Silicon in low concentration and with low surface mobility can be incorporated in solid solution phase(Traverse et al., 2001) (Eriksson et al., 2014), but with increasing concentrations, the Si segregation already occurs with the formation of an amorphous phase of either silicon nitride or free silicon.

With N deficiency and with relatively high Si content, metal silicides can be formed, which are stable at high temperature due to their low vapour pressure and refractory nature. The presence of free Si has been proved to be efficient in the oxidation resistance improvement, as reported by Llauro et al (Llauro et al., 1998) demonstrating that TiNSi codeposits improves the oxidation resistance as compared to CVD TiN, and for greater amount of titanium silicide, it has better improvement of oxidation behavior. The tested samples had 2, 13 and 17 at. % of Si and 45, 35 and 32 at. % of nitrogen, respectively. The amorphous phases are usually better to prevent the layer further oxidation than a polycrystalline layer, where grain boundaries provide a number of diffusion paths for oxygen. With the formation of an amorphous layer the number of diffusion paths decrease considerably leading to the passivation regime (Llauro et al., 1998).

In the design with two absorption layers (high and low absorption layers), it is necessary to adjust the nitrogen content to obtain the desired optical properties. This usually means that the nitride layer is not stoichiometric, having some nitrogen deficiency, resulting that part of the metals atoms are in the metallic oxidation state. In the $AlSiTiN_x$ layer, as shown in section 2.1.3, part of Ti and Si atoms are in metallic oxidation state. In the structure based on WSiAlNx/ WSiAlOyNx layers (A. AL-Rjoub et al., 2018) , the nitride layer exhibited some W atoms in the metallic oxidation state and in the case of absorber stack based on CrAlSiNx/CrAlSiNxOy(AL-Rjoub et al., 2019) absorption layers, the nitride also revealed some Cr and Si atoms in the metallic oxidation state.

The Si content can also play an important role in the performance of this type of coatings. In case of Si addition to CrN, Kim et al(Kim et al., 2006) reported that $Cr_{0.67}Si_{0.33}N$ revealed better oxidation resistance than $Cr_{0.78}Si_{0.22}N$(Kim et al., 2006). The performance of an absorber coating

based on CrAlSiNx/CrAlSiNxOy exhibited a dependence with Si content(A AL-Rjoub et al., 2018) (Al-rjoub et al., 2019) with the best performance for a Si content close to 20 at. % in a nitride with about 27 at.% of nitrogen. The $AlSiTiN_x$/$SiAlTiO_yN_x$ layers have 22 and 25 at.% of Si, respectively, but with the nitride with 33 at. % of nitrogen. The Si and N contents can justify why this design has a better performance than the one based on CrAlSiNx/CrAlSiNxOy. The structure based on WSiAlNx/ WSiAlOyNx layers also exhibited excellent performance. The WSiAlNx layer had 20 at. % of Si and 29 at. % of nitrogen, while the WSiAlOyNx layer had 20 at% of Si. These samples have excellent thermal and chemical stability and have in common a Si content of about 20 at. % the nitride with around 30 at. % of nitrogen(A. AL-Rjoub et al., 2018).

3. Conclusions

A multilayered tandem coating of selective solar radiation absorption for high temperature applications was designed and deposited by dc magnetron sputtering. The stack is based on four layers of structure ($W/AlSiTiN_x/SiAlTiO_yN_x/SiAlO_x$); back reflector/high absorber/low absorber/antireflection layer, respectively. The structural, optical and chemical properties of their single layers were studied. With increasing nitrogen and oxygen partial pressures during deposition, $AlSiTiN_x$ and $SiAlTiO_yN_x$ layers lost their metallic behavior and become more transparent. The increase of the nitrogen and the oxygen contents, induced the formation of Si and Al nitrides and oxynitrides, resulting in a decrement of their optical constants n and k. The two absorbing layers $AlSiTiN_x$ and $SiAlTiO_yN_x$ are amorphous, as confirmed by the XRD analysis. The XPS analyses confirm the formation of metals nitrides, oxynitrides, and oxides bonding. However, the $AlSiTiN_x$, layer has some Ti and Si atoms in metallic oxidation state. The multilayer coating was theoretically designed based on the obtained data from the single layers and then deposited on stainless-steel substrates. The total thickness of as deposited coating is about 302 nm, and shows simultaneously high average solar absorptance, α=95.5 %, and very low emissivity, ε= 9.6 % (calculated for 500 ºC), together with high thermal stability at 500 ºC, in air and at 630 ºC, in vacuum, for 350 h and 220 h, respectively. The thermal emissivity improved for all samples, ensuring that the W back reflector layer maintained its reflectivity and it is well protected by the other top layers. With these excellent results, we strongly recommend this choice of design and materials for high temperature thermal applications, especially for CSP coating for electricity production.

ACKNOWLEDGMENTS

The authors acknowledge the support of FCT in the framework of the Strategic Funding UID/FIS/04650/2013 and the financial support of FCT, POCI and PORL operational programs through the project POCI-01-0145-FEDER-016907 (PTDC/CTM-ENE/2892/2014), co-financed by European community fund FEDER.

The authors are so thankful to Saja Darwish for the English corrections.

References

AL-Rjoub, A., Costa, P., Rebouta, L., Cerqueira, M.F., Alpuim, P., Barradas, N.P., Alves, E., 2017. Characterization of magnetron sputtered sub-stoichiometric CrAlSiNx and CrAlSiOyNx coatings. Surf. Coatings Technol. 328, 134–141. https://doi.org/10.1016/j.surfcoat.2017.08.038

AL-Rjoub, A., Rebouta, L., Costa, P., Barradas, N.P., Alves, E., Ferreira, P.J., Abderra, K., Matilainen, A., Pischow, K., 2018. A design of selective solar absorber for high temperature applications. Sol. energy 172, 177–183. https://doi.org/DOI: 10.1016/j.solener.2018.04.052

Al-rjoub, A., Rebouta, L., Costa, P., Cunha, N.F., Lanceros-mendez, S., Barradas, N.P., Alves, E., 2019. The e ff ect of increasing Si content in the absorber layers (CrAlSiNx/CrAlSiOyNx) of solar selective absorbers upon their selectivity and thermal stability. Appl. Surf. Sci. 481, 1096–1102. https://doi.org/10.1016/j.apsusc.2019.03.208

AL-Rjoub, A., Rebouta, L., Costa, P., Vieira, L.G., 2018. Multi-layer solar selective absorber coatings based on W/WSiAlN x/WSiAlOyNx /SiAlOx for high temperature applications. Sol. Energy Mater. Sol. Cells 186, 300–308. https://doi.org/DOI: 10.1016/j.solmat.2018.07.001

AL-Rjoub, A., Rebouta, L., Costa, P., Vieira, L.G., Miranda, T.M.R., Barradas, N.P., Alves, E., 2019. CrAlSiN barrier layer to improve the thermal stability of W/CrAlSiNx/CrAlSiOyNx/SiAlOx solar thermal absorber. Sol. Energy Mater. Sol. Cells 191, 235–242. https://doi.org/DOI: 10.1016/j.solmat.2018.11.023

Antonaia, A., Castaldo, A., Addonizio, M.L., Esposito, S., 2010. Stability of W-Al_2O_3 cermet based solar coating for receiver tube operating at high temperature. Sol. Energy Mater. Sol. Cells 94, 1604–1611. https://doi.org/10.1016/j.solmat.2010.04.080

Barradas, N.P., Jeynes, C., 2008. Advanced physics and algorithms in the IBA DataFurnace. Nucl. Instruments Methods Phys. Res. B 266, 1875–1879. https://doi.org/10.1016/j.nimb.2007.10.044

Barshilia, H., V. Grips, Rajam, S., 2007. solar selective coating having higher thermal stability useful for harnessing solar energy and a process for the preparation thereof.

Biesinger, M.C., Lau, L.W.M., Gerson, A.R., St, R., Smart, C., 2010. Resolving surface chemical states in XPS analysis of first row transition metals , oxides and hydroxides : Sc , Ti , V , Cu and Zn. Appl. Surf. Sci. 257, 887–898. https://doi.org/10.1016/j.apsusc.2010.07.086

Bogaerts, W.F., Lampert, C., 1983. Review Materials for photothermal solar energy conversion. Mater. Sci. 18, 2847–2875. https://doi.org/10.1007/BF00700767

Cagnoli, M., Froio, A., Savoldi, L., Zanino, R., 2019. Multi-scale modular analysis of open volumetric receivers for central tower CSP systems. Sol. Energy 190, 195–211. https://doi.org/10.1016/j.solener.2019.07.076

Chen, G.S., Yang, L.C., Tian, H.S., Hsu, C.S., 2005. Evaluating substrate bias on the phase-forming behavior of tungsten thin films deposited by diode and ionized magnetron sputtering. Thin Solid Films 484, 83–89. https://doi.org/10.1016/j.tsf.2005.02.032

Chen, H., Zheng, B.C., Li, Y.G., Wu, Z.L., Lei, M.K., 2019. Flexible hard TiAlSiN nanocomposite

coatings deposited by modulated pulsed power magnetron sputtering with controllable peak power. Thin Solid Films 669, 377–386. https://doi.org/10.1016/j.tsf.2018.10.031

Costa, P., AL-Rjouba, A., Rebouta, L., Manninen, N.K., Alves, D., Almeida, B., Barradas, N.P., Alvese, E., 2018. Influence of Al/Si atomic ratio on optical and electrical properties of magnetron sputtered $Al_{1-x}Si_xO_y$ coatings. Thin Solid Films 669, 475–481. https://doi.org/https://doi.org/10.1016/j.tsf.2018.11.036

Dan, A., Jyothi, J., Chattopadhyay, K., Barshilia, H.C., Basu, B., 2016. Spectrally selective absorber coating of WAlN/WAlON/Al_2O_3 for solar thermal applications. Sol. Energy Mater. Sol. Cells 157, 716–726. https://doi.org/10.1016/j.solmat.2016.07.018

Dias, D., Rebouta, L., Costa, P., Al-Rjoub, A., Benelmeki, M., Tavares, C.J., Barradas, N.P., Alves, E., Santilli, P., Pischow, K., 2017. Optical and structural analysis of solar selective absorbing coatings based on AlSiOx:W cermets. Sol. Energy 150, 335–344. https://doi.org/10.1016/j.solener.2017.04.055

Du, M., Liu, X., Hao, L., Wang, X., Mi, J., Jiang, L., Yu, Q., 2013. Microstructure and thermal stability of Al/$Ti_{0.5}Al_{0.5}N$/$Ti_{0.25}Al_{0.75}N$/AlN solar selective coating. Sol. Energy Mater. Sol. Cells 111, 49–56. https://doi.org/10.1016/j.solmat.2012.12.010

Eriksson, A.O., Tengstrand, O., Lu, J., Jensen, J., Eklund, P., Rosén, J., Petrov, I., Greene, J.E., Hultman, L., 2014. Si incorporation in Ti 1−x Si x N films grown on TiN (001) and (001) -faceted TiN (111) columns. Surf. Coat. Technol. 257, 121–128. https://doi.org/10.1016/j.surfcoat.2014.05.043

Fernández-García, A., Zarza, E., Valenzuela, L., Pérez, M., 2010. Parabolic-trough solar collectors and their applications. Renew. Sustain. Energy Rev. 14, 1695–1721. https://doi.org/10.1016/j.rser.2010.03.012

Kalogirou, S., Lloyd, S., Ward, J., 1997. Modelling, optimisation and performance evaluation of a

parabolic trough solar collector steam generation system. Sol. Energy 60, 49–59. https://doi.org/10.1016/S0038-092X(96)00131-4

Kennedy, C.E., 2002. Review of Mid-to High-Temperature Solar Selective Absorber Materials. Natl. Renew. Energy Lab. https://doi.org/10.2172/15000706

Kim, J.W., Kim, K.H., Lee, D.B., Moore, J.J., 2006. Study on high-temperature oxidation behaviors of Cr-Si-N films. Surf. Coatings Technol. 200, 6702–6705. https://doi.org/10.1016/j.surfcoat.2005.10.004

Llauro, G., B, F.G., Sibieude, F., Hillel, R., 1998. Oxidation behavior of CVD TiN – Ti5Si3 composite coatings. Thin Solid Films 315, 336–344. https://doi.org/10.1016/S0040-6090(97)00795-5

Najafi, H., Karimi, a., Alexander, D., Dessarzin, P., Morstein, M., 2013. Effects of Si and Y in structural development of (Al,Cr,Si/Y)O_xN_{1-x} thin films deposited by magnetron sputtering. Thin Solid Films 549, 224–231. https://doi.org/10.1016/j.tsf.2013.06.062

Nuru, Z.Y., Arendse, C.J., Nemutudi, R., Nemraoui, O., Maaza, M., 2012. Pt – Al_2O_3 nanocoatings for high temperature concentrated solar thermal power applications. Phys. B Phys. Condens. Matter 407, 1634–1637. https://doi.org/10.1016/j.physb.2011.09.104

O'Keefe, M.J., Grant, J.T., 1996. Phase transformation of sputter deposited tungsten thin films with A-15 structure. J. Appl. Phys. 79, 9134–9141. https://doi.org/10.1063/1.362584

O'Leary, S.K., Johnson, S.R., Lim, P.K., 1997. The relationship between the distribution of electronic states and the optical absorption spectrum of an amorphous semiconductor : An empirical analysis. Appl. Phys. 82. https://doi.org/10.1063/1.365643

Odeh, S.D., Morrison, G.L., Behnia, M., 1998. Modelling of parabolic trough direct steam generation solar collectors. Sol. Energy 62, 395–406. https://doi.org/10.1016/S0038-092X(98)00031-0

Oliveira, J.C., Fernandes, F., Ferreira, F., Cavaleiro, A., 2015. Tailoring the nanostructure of Ti – Si – N

403 thin fi lms by HiPIMS in deep oscillation magnetron sputtering (DOMS) mode. Surf. Coat. Technol.
404 264, 140–149. https://doi.org/10.1016/j.surfcoat.2014.12.065

405 Rahman, M.M., Jiang, Z., Munroe, P., Chuah, L.S., Zhou, Z., Xie, Z., Yin, C.Y., Ibrahim, K., Amri, A.,
406 Kabir, H., Haque, M., Mondinos, N., Altarawneh, M., Dlugogorski, B.Z., 2016. Chemical bonding
407 states and solar selective characteristics of unbalanced magnetron sputtered $Ti_xM_{1-x-y}N_y$ films
408 Article. RSC Adv. 6, 36373–36383. https://doi.org/10.1039/C6RA02550A

409 Rebouta, L., Capela, P., Andritschky, M., Matilainen, A., Santilli, P., Pischow, K., Alves, E., 2012a.
410 Characterization of TiAlSiN/TiAlSiON/SiO_2 optical stack designed by modelling calculations for
411 solar selective applications. Sol. Energy Mater. Sol. Cells 105, 202–207.
412 https://doi.org/10.1016/j.solmat.2012.06.011

413 Rebouta, L., Pitães, A., Andritschky, M., Capela, P., Cerqueira, M.F., Matilainen, A., Pischow, K., 2012b.
414 Optical characterization of TiAlN/TiAlON/SiO_2 absorber for solar selective applications. Surf. Coat.
415 Technol. 211, 41–44. https://doi.org/10.1016/j.surfcoat.2011.09.003

416 Rebouta, L., Sousa, A., Andritschky, M., Cerqueira, F., Tavares, C.J., Santilli, P., Pischow, K., 2015.
417 Solar selective absorbing coatings based on AlSiN/AlSiON/AlSiOy layers. Appl. Surf. Sci. 356,
418 203–212. https://doi.org/10.1016/j.apsusc.2015.07.193

419 Soum-glaude, A., Le, A., Bichotte, M., Escape, C., Dubost, L., 2017. Optical characterization of TiAlN
420 x/TiAlNy/ Al2O3 tandem solar selective absorber coatings. Sol. Energy Mater. 170, 254–262.
421 https://doi.org/10.1016/j.solmat.2017.06.007

422 Thobor-keck, A., Lapostolle, F., Dehlinger, A.S., Pilloud, D., Pierson, J.F., Coddet, C., 2005. Influence of
423 silicon addition on the oxidation resistance of CrN coatings. Surf. Coat. Technol. 200, 264–268.
424 https://doi.org/10.1016/j.surfcoat.2005.02.029

425 Traverse, A., Vaz, F., Rebouta, L., Girardeau, T., Pacaud, J., Riviere, J.P., 2001. Structural transitions in

426 hard Si-based TiN coatings : the effect of bias voltage and temperature. Surf. Coat. Technol. 147,
427 274–279. https://doi.org/10.1016/S0257-8972(01)01395-0

428 Vepfek, S., Reiprich, S., 1995. A concept for the design of novel superhard coatings. Thin Solid Films
429 268, 64–71. https://doi.org/10.1016/0040-6090(95)06695-0

430 Veprek, S., Veprek-heijman, M.J.G., 2008. Industrial applications of superhard nanocomposite coatings.
431 Surf. Coat. Technol. 202, 5063–5073. https://doi.org/10.1016/j.surfcoat.2008.05.038

432 Wainstein, D., Kovalev, A., 2018. Tribooxidation as a Way to Improve the Wear Resistance of Cutting
433 Tools. Coatings 8,223, 1–9. https://doi.org/10.3390/coatings8060223

434 Wang, X., Gao, J., Hu, H., Zhang, H., Liang, L., Javaid, K., 2017. High-temperature tolerance in WTi-
435 Al2O3 cermet-based solar selective absorbing coatings with low thermal emissivity. Nano Energy
436 37, 232–241. https://doi.org/10.1016/j.nanoen.2017.05.036

437 Wang, X., Luo, T., Li, Q., Cheng, X., Li, K., 2019. High performance aperiodic metal-dielectric
438 multilayer stacks for solar energy thermal conversion. Sol. Energy Mater. Sol. Cells 191, 372–380.
439 https://doi.org/10.1016/j.solmat.2018.12.006

440 Wu, Y., Wang, C., Sun, Y., Ning, Y., Liu, Y., Xue, Y., Wang, W., Zhao, S., Tomasella, E., 2015. Study
441 on the thermal stability of Al / NbTiSiN / NbTiSiON / SiO 2 solar selective absorbing coating. Sol.
442 Energy 119, 18–28. https://doi.org/10.1016/j.solener.2015.06.021

443 Wu, Z.L., Li, Y.G., Wu, B., Lei, M.K., 2015. Effect of microstructure on mechanical and tribological
444 properties of TiAlSiN nanocomposite coatings deposited by modulated pulsed power magnetron
445 sputtering. Thin Solid Films 597, 197–205. https://doi.org/10.1016/j.tsf.2015.11.047

446 Yin, Y., Collins, R.E., 1995. Optimization and analysis of solar selective surfaces with continuous and
447 multilayer profiles. J. Appl. Physiscs 77, 6485. https://doi.org/10.1063/1.359124

448 Zhang, J., Chen, T.P., Liu, Y.C., Liu, Z., Yang, H.Y., 2017. Modeling of a selective solar absorber thin

film structure based on double TiN_xO_y layers for concentrated solar power applications. Sol. Energy 142, 33–38. https://doi.org/10.1016/j.solener.2016.12.012

Zhang, Q., Yin, Y., Mills, D.R., 2006. High efficiency Mo-Al2O3 cermet selective surfaces for high-temperature application. Sol. Energy Mater. Sol. Cells 40, 43–53. https://doi.org/10.1016/0927-0248(95)00078-X

Zhao, S., Wackelgard, E., 2006. The optical properties of sputtered composite of Al – AlN. Sol. Energy Mater. Sol. Cells 90, 1861–1874. https://doi.org/10.1016/j.solmat.2005.11.006

Zou, C., Huang, L., Wang, J., Xue, S., 2015. Effects of antireflection layers on the optical and thermal stability properties of a spectrally selective CrAlN – CrAlON based tandem absorber. Sol. Energy Mater. Sol. Cells 137, 243–252. https://doi.org/10.1016/j.solmat.2015.02.010